Spring 5-2017

Synthesis of Polythioether Nanoparticles via Thiol-alkene/alkyne Photopolymerization in Miniemulsion

Susan E. Walley
University of Southern Mississippi

The University of Southern Mississippi

Synthesis of Polythioether Nanoparticles *via* Thiol-alkene/alkyne Photopolymerization in Miniemulsion

by

Susan E. Walley

A Thesis
Submitted to the Honors College of
The University of Southern Mississippi
in Partial Fulfillment
of the Requirements for the Degree of
Bachelor of Science
in the Department of Polymer Science and High Performance Materials

May 2017

Approved by

_____

Derek Patton, Ph.D., Associate Professor
Polymer Science

_____

Jeffrey Wiggins, Ph.D., Director
Department of Polymers Science and
High Performance Materials

_____

Ellen Weinauer, Ph.D., Dean
Honors College

Abstract

Emulsion-based processes – such as miniemulsion polymerizations – provide well-studied synthetic routes to polymer nanomaterials. Miniemulsion polymerizations are characterized as aqueous dispersions of small, narrowly distributed monomer droplets created through high shear and stabilized against Ostwald ripening/collisional degradation by addition of an appropriate surfactant and costabilizer. In this work, thiol–alkene/alkyne photopolymerization in miniemulsion is demonstrated as a simple, rapid, and one-pot synthetic approach to polythioether nanoparticles with tuneable particle size and clickable functionality. Nanoparticles with mean particle diameters ranging from 45 nm to 200 nm were synthesized through simple modifications to the miniemulsion formulation and processing parameters. Facile access to thiol or alkene/alkyne functional nanoparticles, and subsequent postpolymerization modifications of these functional moieties using thiol-Michael, thiol-yne, and CuAAC click reactions are explored. The strategy is also useful in the synthesis of composite polymer–inorganic nanoparticles such as silver for antimicrobial activity.

Key Terms: Thiol-alkene/alkyne, miniemulsion, nanoparticles, antimicrobial

Acknowledgements

I would like to give my thanks and appreciation to my research advisor, Dr. Derek Patton. Working in the Patton Research Group for the past three years has molded me both as a scientist and a person. Dr. Patton has always been open, supportive, and welcoming of all my endeavors. It truly has been a pleasure to work under his leadership. I would also like to acknowledge all the Patton group for their kindness and helpfulness during my time at Southern Miss.

I also want to thank my parents and friends for their support during my undergraduate research career. Their unwavering support and belief in me helped me continue my path.

Finally, I want to give a special acknowledgement and thanks to my graduate students, Dahlia and Doug Amato. I will never be able to express the gratitude that I have for them. They molded me into the scientist that I am today and have given me the tools and values to continue growing. Working under their guidance comprises some of my fondest memories while at Southern Miss. I will always be thankful that I could work for them.

I would also like to acknowledge the National Science Foundation (Award Number OIA-1430364) and the USM Eagle Scholars Program for Undergraduate Research (Eagle SPUR) for financial support of the research described in this thesis.

Table of Contents

List of Figures

List of Abbreviations

Surfmers	Surfactant monomers
Thiol-ene	Thiol-alkene
Thiol-yne	Thiol-alkyne
HD	Hexadecane
BA	Butyl Acetate
CuAAC	Copper-catalyzed azide–alkyne 1,3-dipolar cycloaddition
NP	Nanoparticle
TTT	1,3,5-Triallyl-1,3,5-triazine-2,4,6(1*H*,3*H*,5*H*)-trione
PETMP	Pentaerythritol tetrakis(3-mercaptopropionate)
Irgacure 184	1-hydroxycyclohexyl phenyl ketone
SDS	Sodium dodecylsulfate
UV	Ultraviolet
DLS	Dynamic light scattering
O/W mixture	Organic/Water mixture
MEHQ	Monomethyl ether hydroquinone
NMR	Nuclear magnetic resonance
TMPTPE	Trimethylolpropane tripropargyl ether
TEM	Transmission electron microscopy
AFM	Atomic force microscopy
T_g	Glass transition temperature
DSC	Differential scanning calorimetry
AgNPs	Silver nanoparticles

Chapter I. Introduction

Polymer nanoparticles with tunable functionality have emerged as a promising and viable technology platform for coatings, cosmetics, nanomedicine, bioimaging, and delivery applications. The prospects of advancing these and other technologies have provided great impetus for the development of rapid, low-cost methodologies for the synthesis of functional polymer nanoparticles – particularly with sizes less than 100 nm. Polymer nanoparticles have been prepared by two general routes: 1) postpolymerization processing, including nanoprecipitation, dialysis, and supercritical fluid expansion, and 2) direct polymerization of monomers or crosslinking of macromers in dispersed heterophase systems, including microfluidics, microemulsion, and miniemulsions.[1] Miniemulsions – with droplet sizes typically in the range of 20-200 nm – are particularly well-suited for the synthesis of small polymer nanoparticles.[2-3]

The overarching goal of this thesis is to elucidate the design parameters necessary for the effective utilization of thiol-ene and thiol-alkyne photopolymerization in miniemulsion. More specifically, this thesis seeks to develop simple synthetic strategies based on thiol-ene/yne photopolymerization in miniemulsion that will enable the fabrication of polythioether nanoparticles with diameters < 100 nm and narrow size distributions. I hypothesize that nanoparticles size and polydispersity can be controlled *via* judicious choice of miniemulsion formulation (i.e. monomer loading, surfactant concentration/structure) and emulsification processing parameters. Additionally, I postulate that the surface functionality of the polythioether nanoparticles can be tailored by exploiting the radical-mediated step polyaddition mechanism using non-stoichiometric monomer ratios. Under such conditions, the excess thiol, alkene, or alkyne would

provide reactive handles on the nanoparticle surface for facile postpolymerization modification processes. Finally, the photopolymerization miniemulsion process will be exploited to prepare polythioether nanoparticles capable of encapsulation and release of hydrophobic payloads. I postulate that the encapsulation efficiency and release kinetics can be directly modulated by tailoring the crosslink density of the polythioether nanoparticles.

Chapter II. Literature Review

II.1. Miniemulsions – Discrete Reactors for Synthesis of Polymer Nanoparticles.

Miniemulsions are thermodynamically unstable heterophase systems created under high shear conditions yielding small, narrowly distributed droplets dispersed in a continuous phase.[4] The droplets are kinetically stabilized against coalescence by the addition of a surfactant and against Ostwald ripening (emulsion degradation) by employing a costabilizer - a fatty alcohol or long chain hydrophobe (e.g. hexadecane). Ostwald ripening occurs due to the difference in Laplace pressure between the small and large droplets, and is a direct consequence of the polydispersity of the droplet size distribution. The costabilizer serves to reduce the rate of monomer diffusion from the small to the larger droplets. Unlike conventional emulsion polymerization, initiation and particle nucleation occur predominately in droplets, which serve as discrete nanoreactors, enabling the preservation of size and composition of each droplet during polymer synthesis as shown in Figure 1.[2]

The formation of a miniemulsion requires the input of energy generally from mechanical devices or from the chemical potential of the components. Commonly, high-energy emulsification methods are employed to achieve the necessary shear conditions, such as

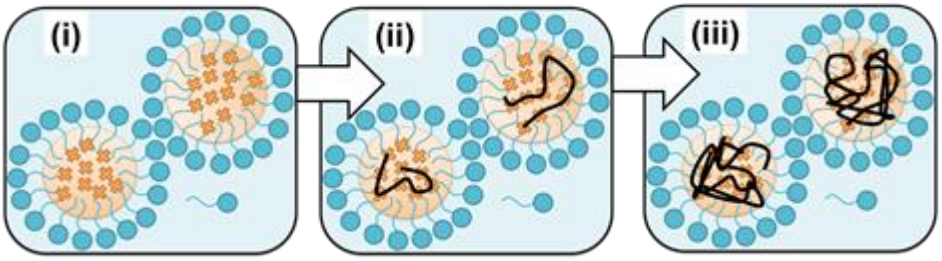

Figure 1 Progression of polymerization in a miniemulsion: (i) initiation, (ii) propagation, and (iii) finally formed nanoparticle. Under appropriate conditions, monomer droplets serve as individual nanoreactors.

high pressure homogenization[5] and acoustic excitation (ultrasonication).[6] High-pressure homogenizers have the highest throughput and are most used in industry, but often require specialized equipment.[4] Ultrasonication is simple and requires minimal equipment, but is often limited to small reaction volumes batches. An additional drawback of ultrasonication is the increase in temperature resulting from the high energy input – an effect that can cause premature polymerization to occur.[7] Membrane emulsification is a low energy alternative to the high energy methods mentioned, and provides tunable droplet sizes with low polydispersities.[8] Membrane emulsification describes a wide variety of techniques – including cross-flow and premix techniques – whereby a dispersed phase is forced through an orifice in a membrane into an immiscible continuous phase, thereby generating an emulsion.[9] In cross-flow membrane processes, the emulsion is formed by the pushing the dispersed phase through a membrane into a cross-flowing continuous phase. The mean droplet size is typically 2–50 times larger than the mean pore size, depending on the choice of the membrane, the cross-flow velocity, the ratio between the two phases, and the transmembrane pressure. In contrast, premix membrane emulsification produces a fine emulsion by extruding or homogenizing a pre-formed coarse emulsion through a membrane pore under pressure. Premix membrane emulsification can be used to prepare miniemulsions with a much smaller mean droplet

size than the mean pore size;[10] however, the particle breakup mechanism in the pre-mix process has not been fully elucidated.

II.2. Step Polyaddition Polymerizations within Miniemulsions.

While miniemulsion polymerizations have predominately been conducted using radical chain growth mechanisms, several examples have highlighted the utility of various step-growth mechanisms – particularly step-growth polyaddition polymerizations.[11-12] The earliest work focused on classic polyaddition reactions in miniemulsion, such as diamine/epoxide[13] and diisocyanates/diols.[14] More recently, the focus has shifted to "click" polyaddition reactions in miniemulsions for the synthesis of polymer microparticles, nanoparticles, and nanocapsules. Landfester *et al.*[15] employed miniemulsion copper-mediated and copper-free azide-alkyne 1,3-dipolar cycloaddition (CuAAC) interfacial polymerization for the synthesis of polytriazole nanocapsules. Similarly, Bernard *et al.*[16] reported interfacial CuAAC miniemulsion polymerization of diazides and dialkynes under microwave irradiation to achieve glyconanocapsules with high conversion (>98%) in under 30 min.

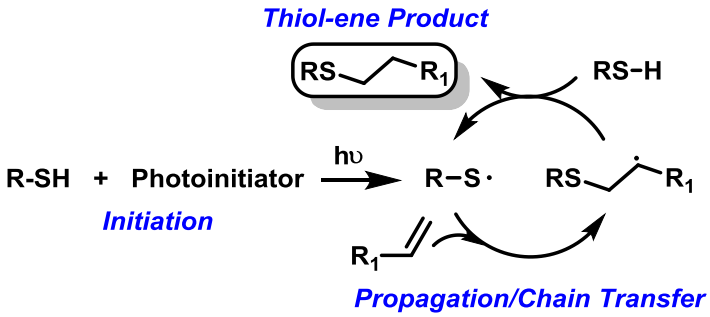

Figure 2. Radical-mediated thiol-ene photopolymerization.

In addition to CuAAC, thiol-mediated chemistries (i.e. thiol-ene/yne, thiol-Michael) represent an attractive family of "click" polyaddition reactions for rapid fabrication of microparticles and nanoparticles in dispersed heterophase systems, as these reactions

generally proceed under mild conditions with high efficiency and rapid reaction kinetics.[17-19] For radical-mediated thiol-ene reactions (Figure 2), the thioether product forms *via* a free-radical step-growth process facilitated by a rapid, highly efficient chain transfer reaction between multifunctional alkenes and thiols, which provides insensitivity to oxygen and water. The earliest examples of thiol-ene related miniemulsions involved surface functionalization of residual alkenes with PEG-thiol on styrene/divinylbenzene composite nanoparticles,[20] and crosslinked biodegradable nanoparticles composed of allyl-functionalized polylactide with a difunctional thiol.[21] Regarding direct polymerization of thiol-ene in disperse heterophase systems, Shipp and coworkers[22] recently reported the first example of crosslinked polythioether microparticles synthesized via thiol-ene suspension photopolymerization. Shipp's initial work focused on the effects of surfactant concentration, co-solvent, and mixing on microparticle formation, while subsequent work explored the dependence of microparticle size and stability on surfactant structure.[23] These initial examples clearly illustrated the utility of thiol-ene photopolymerization for creating microparticles with rapid reaction rates, high monomer conversion and homogeneous network structure in dispersed systems; however, Shipp's work focused minimally on the use of high-energy ultrasonication for the preparation of small thiol-ene nanoparticles. Similarly, Zhang *et al.*[24] reported thiol-ene suspension photopolymerization for the synthesis of large (>200 μm) porous microparticles using PMMA as a porogen. In 2014, Jasinski *et al.*[25] reported thiol-ene photopolymerization in miniemulsion using a difunctional thiol and a difunctional alkene yielding linear poly(thioether ester) nanolatex particles with 130 nm diameter and 55% crystallinity. The authors demonstrated the formation of clear, chemically resistant, and

elastomeric films upon evaporation of water from the cured dispersions. It is also noteworthy to mention recent work by Bowman *et al.*[26] that utilized thiol-Michael polyaddition reactions in dispersion polymerization to fabricate monodisperse microspheres (>1 μm) from multifunctional thiols and Michael acceptors. Bowman importantly showed the ease by which fluorescent microspheres could be prepared *via* postpolymerization modification using off-stoichiometric conditions.

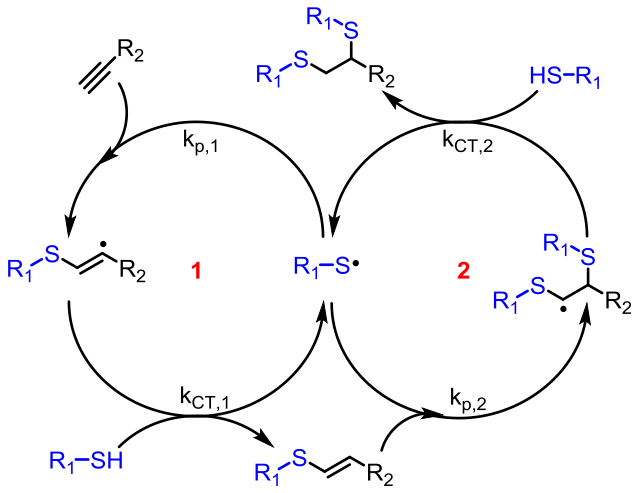

Figure 3. Radical-mediated thiol-alkyne photopolymerization.

Despite many advantages of thiol-ene reactions,[27] thiol-ene photopolymerization fails to provide direct access to polymer nanoparticles with one of the most commonly exploited functional groups in the "click" chemistry toolbox – i.e. the alkyne moiety. Thiol-alkyne photopolymerization provides one such platform to access polymer materials exhibiting alkyne functionality.[28-30] Thiol-alkyne proceeds *via* a radical-mediated step-growth mechanism involving the addition of two thiols across the alkyne; the first addition yields a vinyl sulfide intermediate that subsequently reacts with a second equivalent of thiol to give the dithioether adduct (Figure 3). Thiol-alkyne photopolymerization proceeds at room temperature, in the presence of oxygen, with rapid reaction kinetics, and yields inherently thiol or alkyne functional materials resulting from

the step-growth process – particularly if carried out under non-stoichiometric monomer ratios.[30] In comparison to thiol-ene, thiol-yne typically provides access to materials with higher crosslink densities and improved thermal properties.[31] However, thiol-yne photopolymerization has rarely been exploited for functional particle-based platforms. DuPrez *et al.*[32-33] first applied this concept for synthesis of thiol or alkyne-functionalized microbeads (diameters ≈ 400 μm) *via* microfluidics using stoichiometric excess of pentaerythritol tetra(3-mercaptopropionate) (PETMP) or 1,7-octadiyne, and explored the microbeads as resin supports for solid phase synthesis. Aside from DuPrez's microbead work, there are no methodologies reported in literature that exploit thiol-yne photopolymerization for direct synthesis of functional polymer nanoparticles.[34]

Considering the relatively few examples of thiol-mediated polyadditions in dispersed systems, and the primary focus of these works on either microparticles or linear nanolatex particles, a significant opportunity remains to exploit thiol-mediated polyadditions in miniemulsion for the fabrication of crosslinked, functional polymer nanoparticles.

II3. Encapsulation and Delivery using Solid Polymer Nanoparticles

Encapsulation of drugs within nanoparticles synthesized *via* thiol-ene/yne chemistry has yet to be demonstrated in literature. Roughly 40% of small molecules considered to be new drug candidates are hydrophobic with poor water solubility.[35] Full exploitation of the therapeutic potential of these drugs relies on solubilization in nontoxic, biocompatible, and/or biodegradable formulations that protect the drugs during transportation, and release at appropriate rates at the site of the target tissue.[36] The last several decades have produced an astounding number of nanoparticle-based drug delivery

systems – including liposomes, dendrimers, polymer conjugates, polymeric micelles and vesicles, hydrogels, solid polymer nanogels, inorganic nanoparticles, and organic/inorganic hybrid nanoparticles.[37-38] Nanoparticle-based delivery systems offer the possibility of (1) optimizing pharmaceutical and pharmacological characteristics of drugs; (2) extending blood circulation duration and enhanced permeation and retention (EPR) within tumor tissues; (3) enhancement of therapeutic efficacy via tissue-, cell-, and cell organelle-specific targeted delivery; (4) possibility of overcoming multidrug resistance of certain types of diseased cells; and (5) co-delivery of multiple therapeutic drugs and imaging agents over the same nanoparticle scaffold. Among the nanoparticle-based systems previously mentioned, nanostructured self-assembled aggregates from amphiphilic block copolymers have been most frequently explored as delivery vehicles. However, tedious synthetic procedures, difficulty in scale-up, variable encapsulation capacities, and premature drug release during transportation/circulation (i.e. critical micelle concentration dependence) are often cited as disadvantages of block copolymer micellar systems.[39]

Solid polymer nanoparticles (SNPs) have received much less attention in the drug delivery literature.[38] SNPs, as the name implies, have a solid core, or at least the core of the nanoparticle forms a macroscopic solid at room temperature. SNPs are often fabricated from biocompatible and/or biodegradable polymers – where active compounds can be firmly adsorbed at their surface, entrapped or dissolved in the matrix. The payload can be released by erosion or degradation of the polymer matrix, by diffusion of the active component from the intact polymer core, or *via* a combination of both processes. As a nanoparticle delivery platform, SNPs offer numerous advantages –

including facile synthetic and encapsulation methodologies (i.e. nanoprecipitation, electrospray techniques, etc.), concentration-independent particle stability, good potential for surface modification and functionalization with various ligands, and the capability to encapsulate and deliver a plethora of therapeutic agents. Given these advantages, there are significant opportunities to impact the field of encapsulation and delivery by employing the combination of thiol-ene/yne photopolymerization and miniemulsion.[27, 34]

Chapter III. Experimental

III.1 Materials for Thiol-ene Nanoparticles

Hexadecane, 1,3,5-triallyl-1,3,5-triazine-2,4,6 (1H, 3H, 5H) trione (TTT), 4-p-methoxy phenol (MEHQ), sodium dodecyl sulfate (SDS), 2,2-dimethoxy-2-phenylacetophenone (DMPA), tetrahydrofuran (THF), 7-mercapto-4-methylcoumarin and butyl acetate (Sigma-Aldrich), pentaerythritol tetra(3-mercaptopropionate) (PETMP, BrunoBock), 1-hydroxycyclohexyl phenyl ketone (Irgacure 184, CIBA), and Texas Red® C2 maleimide (Invitrogen) were obtained at the highest purity available and used without further purification unless otherwise specified.

III.2 General Sample Preparation

Each sample was prepared in a 20-mL scintillation vial with a total volume 10-mL. The organic stock solution shown in Table 1 was added into the vial containing a stock solution of SDS and deionized water. The samples were then placed into an ice bath.

Table 1. General formulation of organic stock solution for thiol-ene photopolymerization in miniemulsion.

Organic Fraction	*Mass (g)*	*Wt. %*
Hexadecane	*0.439 (1.94 mmol)*	*4.72*
TTT	*1.52 (6.10 mmol)*	*16.3*
PETMP	*2.22 (4.53 mmol)*	*23.8*
Irgacure 184®	*0.100 (0.49 mmol)*	*1.07*
4-p-methoxy phenol	*0.030 (0.24 mmol)*	*0.322*
Butyl acetate	*5.00 (43.04 mmol)*	*53.7*

and sonicated using a Q-700A-110 probe ultrasonicator at 5-25% amplitude for 5-45 minutes. The miniemulsions were then cured using an Omnicure S1000-1B with a 100W mercury lamp (λ_{max}=365 nm, 320-500 nm filter) and an intensity of 185 mW/cm^2 for 10 minutes unless noted otherwise. All samples were made in triplicate to ensure reproducible data. To optimize the formulation for small nanoparticles, the organic fraction was varied with a constant SDS concentration of 20 mM. The SDS stock formulation and tabulated samples prepared are listed in Table SI-1 and SI-2.

III.3. Preparation of nanoparticles with excess thiol and excess alkene

Nanoparticles with excess thiol were prepared using a 1.5:1 thiol to alkene stoichiometry, for example, PETMP (2.8 g, 5.73 mmol) and TTT (0.95 g, 3.81 mmol). The remaining constituents in the organic formulation from Table 1 were held constant. To the scintillation vial, 250 µL of organic solution was pipetted into 9.75 mL of 20 mM SDS in DI water. The sample was then ultrasonicated for 20 minutes at 10% amplitude and cured under UV light for 10 minutes. Nanoparticles containing excess alkene were similarly synthesized using a 2:1 alkene to thiol ratio, i.e. TTT (2.15 g, 8.63 mmol) and PETMP (1.58 g, 3.23 mmol).

III.4. Fluorescent tagging of excess thiol nanoparticles

From the nanoparticle suspension (10 mL) with excess thiol prepared in 2.3, 2 mL were removed and placed into a 20-mL scintillation vial wrapped in aluminum foil with a stir bar. A stock solution of Texas Red® C2 maleimide was made by addition 10 µL of Texas Red® C2 maleimide to 100 µL of DMSO. 50 µL of the Texas Red® C2 maleimide stock solution was added to the nanoparticles and stirred overnight. The nanoparticles were purified by centrifugation (5 minutes at 13,300 rpm, Fisher

Scientific™ accuSpin™ Micro 17 centrifuge) to remove unreacted Texas Red® C2 maleimide. The supernatant was removed and the nanoparticle pellet was re-suspended in 1 mL DI water. The nanoparticle suspension was then cast onto a glass slide and allowed to dry at room temperature. The resulting slide was analyzed using a Zeiss LSM 510 confocal laser scanning microscope (λ_{ex}=543 nm).

III.5. Fluorescent tagging of excess alkene nanoparticles

From the nanoparticle suspension (10 mL) with excess ene prepared in 2.3, 1 mL was removed and centrifuged for 18 min at 13,300 rpm. The supernatant was removed and the nanoparticle pellet was re-suspended in 1 mL of THF. A solution was prepared containing 80 mg of 7-Mercapto-4-methylcoumarin, 30 mg of DMPA and 1 mL of THF was added. The solutions were combined and exposed to UV light for 5 minutes to induce the radical thiol-ene reaction. The solution was centrifuged for 10 minutes, supernatant removed, the pellet re-suspended in THF. The coumarin-functionalized nanoparticles were then cast onto a glass slide with a coverslip for analysis by confocal laser scanning microscopy (λ_{ex}=405 nm).

III.6. Materials for Thiol-Alkyne Nanoparticles

Hexadecane, 4-p-methoxy phenol, sodium dodecyl sulfate (SDS), 1,7-octadyne, 1-hexyne, 2,2-dimethoxy-2-phenylacetophenone (DMPA), tetrahydrofuran (THF), 7-mercapto-4-methylcoumarin, sulforhodamine B, silver nitrate ($AgNO_3$), sodium borohydride (NaBH4, ≥96% purity), dodecanethiol (DDT, ≥98% purity), ethanol (EtOH, ACS reagent grade), toluene and butyl acetate (Sigma-Aldrich), pentaerythritol tetra(3-mercaptopropionate) (PETMP, BrunoBock), 1-hydroxycyclohexyl phenyl ketone (Irgacure 184, CIBA), 7-methoxy-4-methylcoumarin (TCI, Tokyo, Japan) and Texas

Red® C2 maleimide (Invitrogen) Click-iT® EdU Imaging Kit with Alexa Fluor® 488 Azide (Life Technologies™) were obtained at the highest purity available and used without further purification unless otherwise specified.

III.6. General Preparation for Thiol-Alkyne Nanoparticles

Each sample was prepared in a 20 mL scintillation vial with a total volume 10 mL. The organic stock solution shown in Table 2 was added into the vial containing a stock solution of SDS and deionized water. The samples were then placed into an ice bath and sonicated using a Q-700A-110 probe ultrasonicator at 20 % amplitude for 20 minutes.

Table 2. General formulation of organic stock solution for thiol-yne photopolymerization in miniemulsion.

Organic Fraction	Mass (g)	Wt. %
Hexadecane	0.5 (2.2 mmol)	7.32
1,7 Octadiyne	0.5 (4.7 mmol)	7.32
PETMP	2.3 (4.7 mmol)	33.67
Irgacure 184	0.1 (0.49 mmol)	1.46
4-p-methoxy phenol	0.03 (0.24 mmol)	0.44
n-butyl acetate	3.4 (29 mmol)	49.78

The miniemulsions were then cured using an Omnicure S1000-1B with a 100W mercury lamp (λ_{max}=365 nm, 320-500 nm filter) and an intensity of 185 mW/cm^2 for 10 minutes unless noted otherwise. All samples were made in triplicate to ensure reproducible data. To optimize the formulation for small nanoparticles, the organic fraction was varied with a constant SDS concentration of 20 mM.

III.7. Preparation of thiol-alkyne nanoparticles with excess thiol and excess alkyne

Nanoparticles with excess thiol were prepared using a 3.2:1 thiol to alkyne stoichiometry, for example, PETMP (3.68 g, 7.531 mmol) and 1,7-octadiyne (0.50 g, 4.7 mmol). The remaining constituents in the organic formulation from Table 1 were held constant. 250 µL of organic solution was pipetted into 9.75 mL of 20 mM SDS in DI water. The sample

was then ultrasonicated for 20 minutes at 10% amplitude and cured under UV light for 10 minutes. Nanoparticles containing excess alkyne were synthesized similarly using a 1.51:1 alkyne to thiol ratio, i.e. 1,7-octadiyne (0.758 g, 7.14 mmol) and PETMP (2.30 g, 4.71 mmol).

III.8. Fluorescent tagging of thiol-alkyne nanoparticles with excess thiol groups.

From the nanoparticle suspension (10 mL) with excess thiol prepared in 1.3, 2 mL were removed and placed into a 20 mL scintillation vial wrapped in aluminum foil with a stir bar. A stock solution of Texas Red® C2 maleimide was made by the addition of 10 µL of Texas Red® C2 maleimide to 100 µL of DMSO. 50 µL of the Texas Red® C2 maleimide stock solution was added to the nanoparticles and stirred overnight. The nanoparticle were purified by centrifugation (5 minutes at 13,300 rpm, Fisher Scientific™ accuSpin™ Micro 17 centrifuge) to remove unreacted Texas Red® C2 maleimide. The supernatant was removed and the nanoparticle pellet was re-suspended in 1 mL DI water. The nanoparticle suspension was then suspended in glycerol on a glass slide and a coverslip was affixed and imaged immediately. The resulting slide was analyzed using a Zeiss LSM 510 confocal laser scanning microscope.

III.9. Fluorescent tagging of thiol-alkyne nanoparticles expressing excess alkyne *via* 7-mercapto-4-methylcoumarin

From the nanoparticle suspension (10 mL) with excess yne prepared in 1.3, 1 mL was removed and centrifuged for 18 min at 13,300 rpm. The supernatant was removed and the nanoparticle pellet was re-suspended in 1 mL of THF. A solution was prepared containing 21 mg of 7-mercapto-4-methylcoumarin, 30 mg of DMPA and 1 mL of THF was added. The solutions were combined and exposed to UV light for 5 minutes to

induce the radical thiol-ene reaction. The solution was centrifuged for 10 minutes, supernatant removed, the pellet re-suspended in THF. The coumarin-functionalized nanoparticle were then cast onto a glass slide with a drop of glycerol and a coverslip for analysis by confocal laser scanning microscopy.

III.10. Fluorescent tagging of thiol-alkyne nanoparticles expressing excess alkyne *via* Alexa Fluor® 488 Azide

From the nanoparticle suspension (10 mL) with excess yne prepared in 1.3, 2 mL were removed and placed into a 20 mL scintillation vial wrapped in aluminum foil with a stir bar. The 1X Click-iT® EdU buffer was prepared with 1.0 mL of dH_2O to the Click-iT® EdU vial. To the Alexa Fluor® 488 vial, 100 µL of Click-iT® reaction buffer, 800 µL of $CuSO_4$ solution, and 100 µL of the prepared 1X Click-iT® reaction buffer was added. From this, 500 µL of the reaction cocktail was added to the nanoparticle suspension and allowed to react overnight. The solution was then centrifuged (10 minutes at 13,300 rpm, Fisher Scientific™ accuSpin™ Micro 17 centrifuge), supernatant removed, nanoparticles resuspended in 1 mL of H_2O and then added to a slide with glycerol. A coverslip was placed on top and was immediately imaged using a Zeiss LSM 510 confocal laser scanning microscope.

III.11. Preparation of hydrophobically modified silver nanoparticle

Dodecanthiol capped AgNPs were prepared using a modified procedure.[40] Briefly, a 2.25 mM stock solution of $AgNO_3$ was prepared with 19.11 mg $AgNO_3$ in 50 mL of EtOH. A second 69.4 mM solution of $NaBH_4$ was prepared with 0.2625 g in 100 mL of EtOH. Into a 20 mL scintillation vial, 14 mL of $NaBH_4$ stock with 25.7 µL of DDT with a magnetic stirbar. The solution was stirred and in one continuous addition, 4 mL of $AgNO_3$ stock

was added, upon which the solution immediately turned yellow and gradually turned dark brown. The solution was centrifuged at 8500 rpm for 12 minutes, supernatant removed, 20 mL EtOH added three times. The final solution was resuspended in varying amounts of either toluene or butyl acetate to adjust the concentration of AgNPs.

III.12. Preparation of composite thiol-alkyne Ag nanoparticles

Each sample was prepared by mixing 250 µL of the 2:1 SH:yne octadiyne formulation with 50 µL of AgNPs (3% wt AgNP solution in butyl acetate). The solution was pipetted up and down to ensure mixing, upon which 250 µL was dispersed in a solution of SDS and deionized water. The samples were placed into an ice bath and were sonicated using a Q-700A-110 probe ultrasonicator at 20 % amplitude for 20 minutes. The miniemulsions were then cured using an Omnicure S1000-1B with a 100W mercury lamp (λ_{max}=365 nm, 320-500 nm filter) and an intensity of 185 mW/cm^2 for 10 minutes.

III.13. Characterization

The size and distribution of the nanoparticles were measured by dynamic light scattering (DLS) using a Microtrac Nanotrac Ultra NPA150. Particle size and distribution were obtained using the Microtrac Flex software (v.10.6.1), which employs non-negatively constrained least-squares (NNLS) and cumulants analysis to obtain the intensity-weighted "z-average" mean particle size as the first cumulant, and the polydispersity index from the second cumulant.[41] Transmission electron micrographs (Digital Imaging with Gatan Model 785 ES1000W Erlangshen CCD Camera) were taken with a Zeiss 900 TEM operating at 50kV. Samples were applied to 200 mesh copper grids (3.05 mm, 200 lines/inch square mesh, EMS Cat. #G200-Cu) coated with Formvar (5% polyvinyl formal resin). The samples were then stained using OsO_4. Atomic force microscopy (AFM) was

performed using a Bruker Icon in tapping mode. The samples were imaged with T300R-25 probes (Bruker AFM Probes) with a spring constant of 40 N m^{-1}. ^{1}H NMR was recorded on a Varian Mercury Plus 300 MHz NMR in D_2O. FTIR was conducted using a Nicolet 8700 spectrometer with a KBr beam splitter and a liquid nitrogen cooled MCT/A detector.

Chapter IV. Results and Discussion

IV.1. Thiol-ene photopolymerization in miniemulsion.

Thiol-ene miniemulsions were prepared initially by adding an organic phase containing multifunctional alkene and thiol monomers, photoinitiator, hydrophobe, inhibitor, and solvent to an aqueous phase consisting of water and surfactant. Figure 4 shows the specific chemical structures used as a model formulation, including pentaerythritol tetra(3-mercaptopropionate) (PETMP) and 1,3,5-triallyl-1,3,5-triazine-2,4,6 (1H, 3H, 5H) trione (TTT) as monomer pairs, 2,2-dimethoxy-2-phenylacetophenone (DMPA) as photoinitiator, sodium dodecyl sulfate (SDS) as surfactant, and hexadecane as the hydrophobe. Our preliminary experiments with this formulation have shown the need for a radical inhibitor to prevent premature polymerization during the emulsification process, thus 4-*p*-methoxy phenol (MEHQ) will be used for this purpose. The miniemulsion was be prepared *via* high-energy ultrasonication, as shown in Figure 4. An ultrasonic horn was inserted into a glass scintillation vial containing the organic monomer phase and an aqueous solution of surfactant. The emulsification process was carried out at 20 kHz, while varying the ultrasonic amplitude and processing time to achieve a steady-state monomer droplet size. Monomer droplet size was followed as a function of ultrasonic processing parameters using dynamic light scattering (DLS) to identify the steady-state

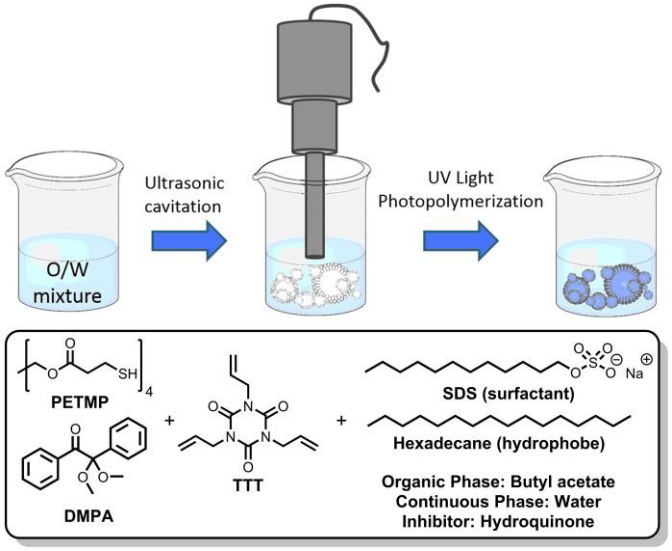

Figure 4. Thiol-ene precursors and miniemulsion process for preparing sub-100 nm polythioether nanoparticle *via* photopolymerization.

droplet size for a given thiol-ene formulation. Upon achieving the steady-state, the monomer droplets were converted to polymer nanoparticles *via* UV-induced photopolymerization. The steady-state monomer droplet size was compared with the polymer nanoparticle size *via* DLS to ensure the efficiency of the miniemulsion templating process.

Initial attempts to synthesize thiol-ene nanoparticles using probe ultrasonication under conditions described in the literature (i.e. in the absence of radical inhibitor as reported by Shipp *et al.*[22]) resulted in the formation of solids in solution and on the surface of the horn during ultrasonication, prior to exposure to UV light, presumably due to thermally-induced polymerization. Because of these observations, I introduced a radical inhibitor – monomethyl ether hydroquinone (MEHQ) – into the organic phase and investigated the effect of inhibitor concentration on the miniemulsion process. MEHQ was chosen because it is a commonly used stabilizer for alkene containing monomers. The MEHQ concentration in the organic phase was varied, where the minimum

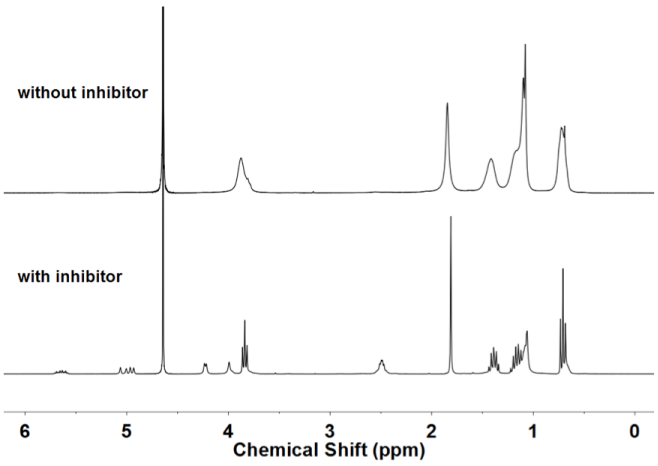

Figure 5. NMR spectra of thiol-ene miniemulsion formulation with and without inhibitor.

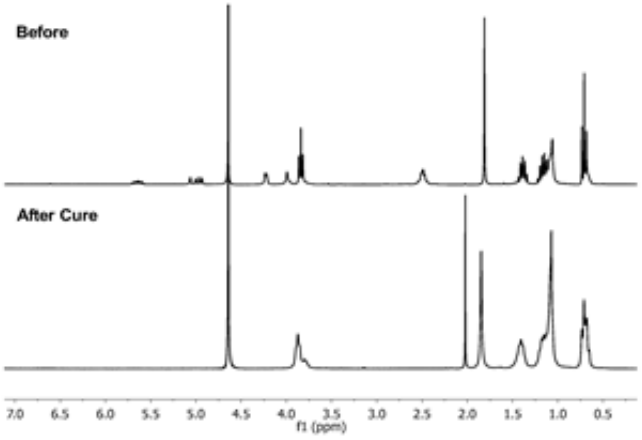

Figure 6. NMR spectra of thiol-ene miniemulsion formulation before and after cure.

concentration that inhibited latex formation was found to be 55.7 mM. MEHQ concentrations below this minimum threshold resulted in the formation of solids on the surface of the ultrasonic horn. To further probe the ability of the inhibitor to prevent premature polymerization during the emulsification process, thiol-ene miniemulsions with and without inhibitor were prepared using a deuterium oxide/SDS solution as the continuous phase. Upon ultrasonication, an aliquot of sample was removed and analyzed *via* ^{1}H NMR, while the remaining fraction of the sample was photopolymerized under UV light prior to collecting a second aliquot for analysis. Figure 5 shows the NMR

spectra of thiol-ene miniemulsions with and without MEHQ prior to UV exposure. The sample with MEHQ showed the typical proton resonances for the unreacted alkene of TTT at 4.92–5.15 ppm and 5.58–5.75 ppm, and a resonance for an unreacted mercaptopropionate (-CH_2CH_2-SH) at 2.51 ppm. Without MEHQ, the miniemulsion formulation exhibited complete disappearance of the alkene and thiol monomer peaks, and displayed peak broadening as an indicator of polymerization. These results provide evidence that the uninhibited sample undergoes polymerization during ultrasonic cavitation process, and that MEHQ is required to prevent premature polymerization. It is also important to note that the inhibitor had a minimal effect on the process of thiol-ene photopolymerization for nanoparticle formation. As shown in Figure 6, in the presence of UV light, the inhibited thiol-ene miniemulsions proceeded to high monomer conversion (>99%) as indicated by complete disappearance of the peaks associated with the thiol and alkene functional groups in NMR of the cured samples.

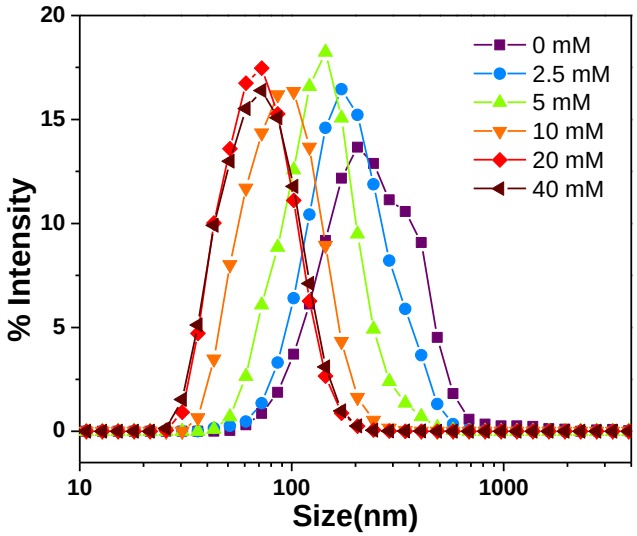

Figure 7. Effect of SDS concentration on nanoparticle size distribution. (Synthetic conditions: 2.5 wt.% organic, 20 min ultrasonication at 10% amplitude, 10 min UV exposure).

The stability and size of monomer droplets, and ultimately polymer nanoparticles, obtained from heterogeneous miniemulsion polymerizations are strongly influenced by several formulation parameters, including surfactant structure and concentration, organic phase weight fraction, and the presence of a costabilizer. To explore the effect of SDS concentration on nanoparticle size, the concentration of SDS was varied from 0 to

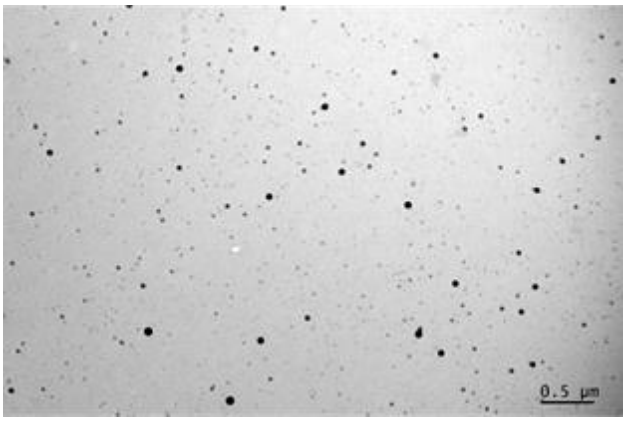

Figure 8. TEM image of thiol-ene nanoparticles.

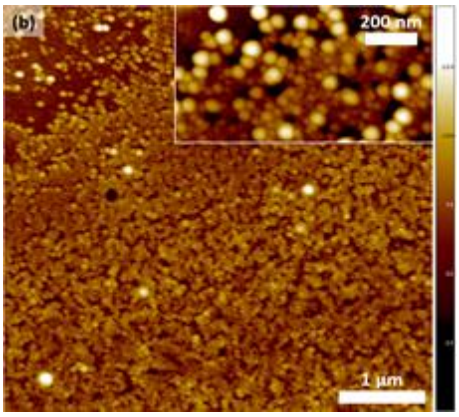

Figure 9. AFM image of thiol-ene nanoparticles.

40 mM, while keeping the organic weight fraction and composition constant. As shown in Figure 7, thiol-ene miniemulsions carried out in the absence of SDS provided a mean particle size of 145 nm and a broad, multimodal particle size distribution (PDI— 0.338). With increasing SDS concentration, the mean particle size systematically decreased due to an increase in surfactant interfacial area and a decrease in interfacial tension enabling

stabilization of smaller nanodroplets. 20 – 40 mM SDS provided thiol-ene nanoparticles with a mean particle size of 55 nm and relatively narrow particle size distributions (PDI: 0.255). Figure 8 shows an image of the thiol-alkene nanoparticles taken by transmission electron microscopy (TEM). Figure 9 shows an image of the same nanoparticles taken by atomic force microscopy (AFM). These images show the successful synthesis of small nanoparticles with sizes ranging from 60-200 nm and are in good agreement with the DLS results. The effect of organic weight fraction on the particle size was also investigated. For these experiments, the concentration of SDS was kept constant (20 mM), while the organic weight fraction is varied from 0.5 – 5 wt. % relative to the aqueous phase. The results from these experiments are shown in Figure 10, which relate mean particle size to the organic weight fraction. The smallest mean particle size (46 nm) was obtained from a system containing 2.5 wt. % organic phase. The corresponding TEM image for the 2.5

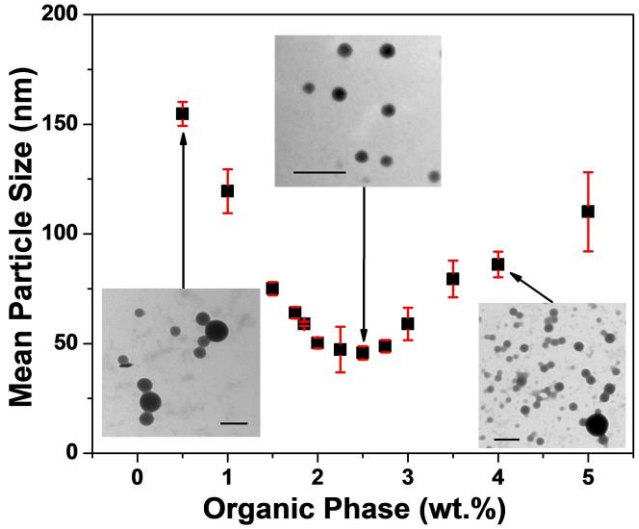

Figure 10. Dependence of the nanoparticle size on (a) organic weight fraction. The insets show representative TEM images of UV cured miniemulsions at various organic weight fractions (scale bar length = 200 nm). (Synthetic conditions: 20 min ultrasonication at 10% amplitude, 10 min UV exposure).

wt. % sample shows well-defined thiol-ene nanoparticles with sizes that are in good agreement with values obtained by DLS. Increasing the organic weight fraction from 2.5 wt. % resulted in an increase in the mean particle size, as shown in Figure 8. The observation of larger particle sizes with increasing organic fraction is likely due to depletion of SDS required to stabilize the smaller nanodroplets.[5] Likewise, decreasing the organic weight fraction from 2.5 wt. % resulted in an increase in nanoparticle size (up to 155 nm at 0.5 wt. %). Destabilization and coalescence of small droplets may be caused by attractive forces between multiple nanodroplets in the presence of excess surfactant – a phenomenon that follows a similar mechanism as described in depletion flocculation.[42-43] While these results clearly demonstrate the feasibility of thiol-ene nanoparticle synthesis at low solids content (i.e. < 5 wt. %), we recognize the need to obtain nanoparticles at high solids content to produce practical nanoparticle yields.

IV.2. Synthesis of thiol and alkene/alkyne functional nanoparticles using non-stoichiometric monomer ratios.

An outstanding feature that ascends from the step-growth radical mechanism of thiol-ene photopolymerization is the capacity to alter the reaction stoichiometry to achieve thiol-ene networks containing either excess thiol or alkene. The excess functional groups arising from non-stoichiometric photopolymerization conditions are then readily available for subsequent functionalization. As illustrated in Figure 11, we used non-stoichiometric ratios of PETMP and TTT – monomers that do not readily undergo homopolymerization – to synthesize sub-100 nm thiol-ene nanoparticles with thiol or alkene functional surfaces in a one-step process. Using similar formulations as previously described, the ratio of thiol to alkene was adjusted to either 2:1 for thiol functionalized

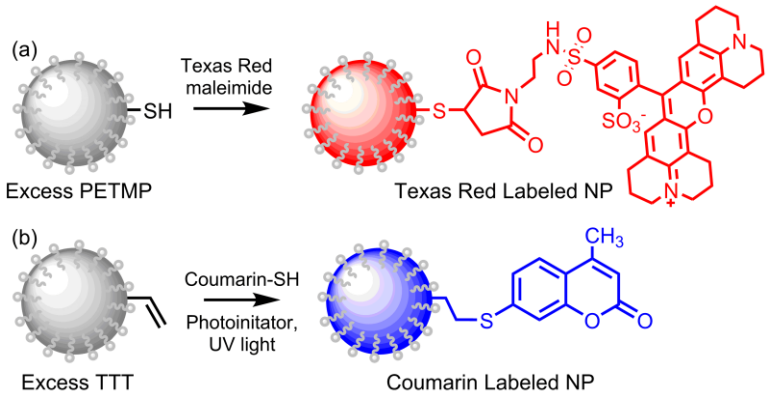

Figure 11. Postpolymerization modification of polythioether nanoparticles prepared with stoichiometric excess thiol or excess alkene *via* (a) thiol-Michael addition with Texas Red maleimide and (b) radical-mediated thiol-ene addition with 7-mercapto-4-methylcoumarin.

functionalized nanoparticles, or 1:2 for alkene functionalized nanoparticles. These formulations were ultrasonicated to create the miniemulsion and photopolymerized, as described previously for stoichiometric samples. Thiol and alkene functionalized nanoparticles were analyzed by solution ^{1}H NMR to confirm the presence of excess thiol and alkene present. Figure 12 shows the NMR spectroscopy results from adding the thiol monomer in excess to ensure the synthesis of thiol-functional nanoparticles. Figure 12 overlays four different NMR spectra: 1) NMR of the alkene monomer, TTT, 2) NMR of the thiol monomer, PETMP, 3) NMR of the solution after sonication, and 4) NMR of the solution after the photopolymerization process. The top plot shows TTT monomer has a peak attributed to the alkene around 5.0 and 5.5 ppm. The second plot shows the thiol monomer has a peak attributed to the thiol around 2.5 ppm. The third spectrum shows the results after the sonication process and shows that the alkene peak was depleted appreciably, while the peak for the thiol remains prominent. The last spectrum shows the results after the curing process. A normal 1:1 monomer ratio NMR plot would show no peaks for the alkene or thiol monomers. However, since the stoichiometry was adjusted

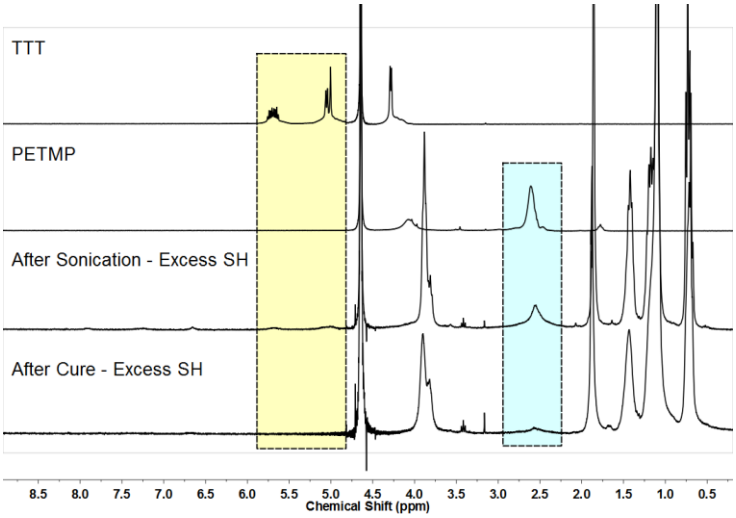

Figure 12. 1H NMR of TTT and PETMP starting materials, miniemulsion containing excess PETMP (2:1 thiol:ene) prior to UV exposure, and miniemulsion containing excess PETMP after UV exposure. The lower spectrum confirms the presence of thiol (~ 2.5 ppm) remaining on the nanoparticles, and the complete consumption of the alkene.

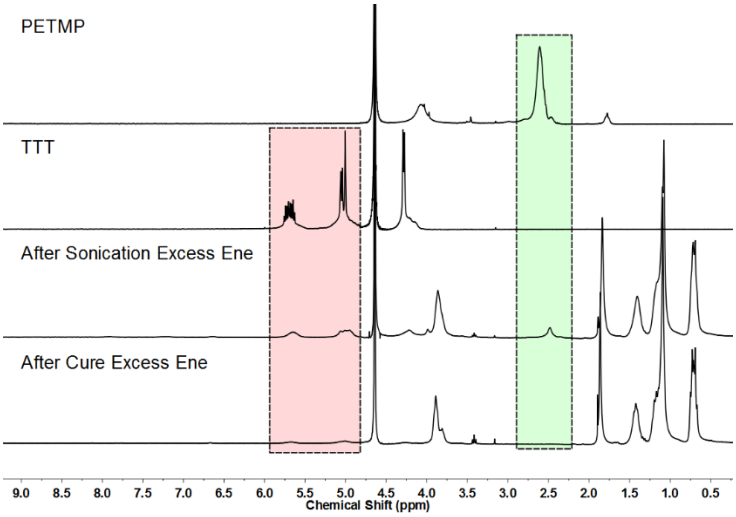

Figure 13. [1]H NMR of TTT and PETMP starting materials, miniemulsion containing excess TTT (1:2 thiol:ene) prior to UV exposure, and miniemulsion containing excess TTT after UV exposure. The lower spectrum confirms the presence of alkene (5.0 – 5.8 ppm) remaining on the nanoparticles, and the complete consumption of the thiol at 2.5 ppm.

to have thiol in excess, the spectrum shows no proton peak for the alkene monomer indicating that the alkene had fully reacted. In the same spectrum, a small peak at 2.5 ppm indicates residual thiol. These results suggest the successful synthesis of thiol-

functional nanoparticles. Similar conclusions can be drawn from Figure 13 for photopolymerizations carried out in the presence of excess alkene monomer.

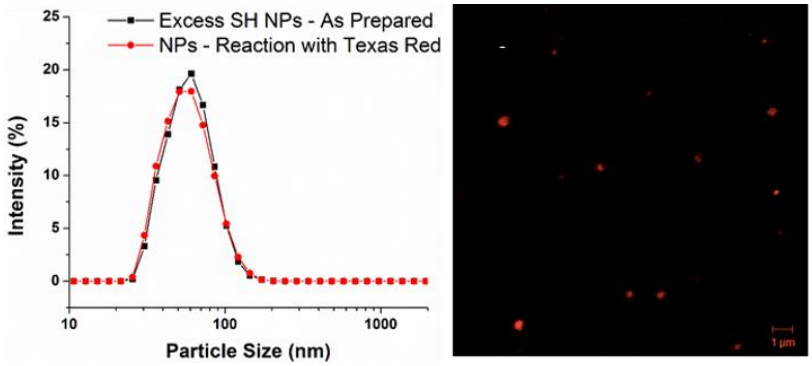

Figure 14. (left) Comparison of particle size with and without Texas Red. (right)Confocal image confirming attachment of Texas Red.

To capitalize on this functionality, the thiol-functional nanoparticles were further reacted with Texas Red maleimide *via* thiol-Michael addition following the reaction scheme in Figure 11a. Figure 14 shows the DLS results for excess thiol nanoparticles before and after reaction with Texas Red. The intensity of the nanoparticles only varies slightly at certain sizes, but overall, the DLS distribution curves are very similar. This result indicates that the influence of the postmodification reaction with Texas Red on the nanoparticle size and aggregation was negligible. Figure 16 shows an image taken by confocal microscopy. The Texas Red will illuminate under a certain wavelength, which is 615 nm. This image proves that the whole of the nanoparticle is reacted with the Texas Red.

After successfully exploiting the functionality of thiol-functional nanoparticles, a similar experiment was conducted to synthesize alkene-functional nanoparticles. This was done by adding the alkene monomer (TTT) in excess and then reacting the alkene-functional nanoparticle with 7-mercapto-4-methylcoumarin following the reaction

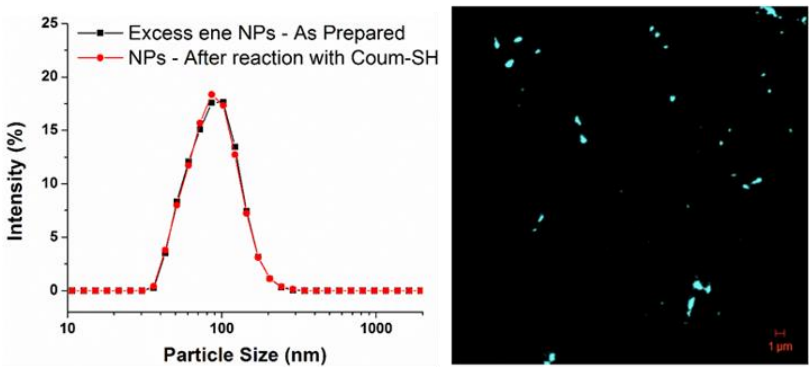

Figure 15. (left) Comparison of particle size with and without coumarin. (right) Confocal image confirming attachment of coumarin.

scheme in Figure 11b. The results from DLS and confocal microscopy are shown in Figure 15. The effect of the postmodification reaction with coumarin on the size and intensity of the nanoparticles are nearly negligible. Confocal imaging was utilized to show full reaction of the alkene-functional nanoparticles with the Coumarin at 385 nm.

IV.3. Thiol-alkyne photopolymerization in miniemulsion.

A transition from thiol-ene to thiol-alkyne photopolymerization enables the synthesis of polythioether nanoparticles with higher crosslink densities, which could lead to better performance properties for applications within the coating, cosmetic, and biomedical industries. Using similar synthetic strategies described for thiol-ene miniemulsions in IX.1, a parallel study using thiol-yne chemistry was performed to explore thiol-yne photopolymerization in miniemulsion. As shown in Figure 16, thiol-alkyne miniemulsions were prepared from an organic solution comprised of photoinitiator, hydrophobe, inhibitor, thiol and alkyne monomers. Three different alkyne monomers, including 1-hexyne, 1,7-octadiyne, and trimethylolpropane tripropargyl ether (TMPTPE) were used with pentaerythritol tetra(3-mercaptopropionate) as the thiol monomer. The organic solution wad then added to an aqueous solution of deionized water and surfactant, sodium dodecyl sulphate. The samples were placed in an ice bath, sonicated,

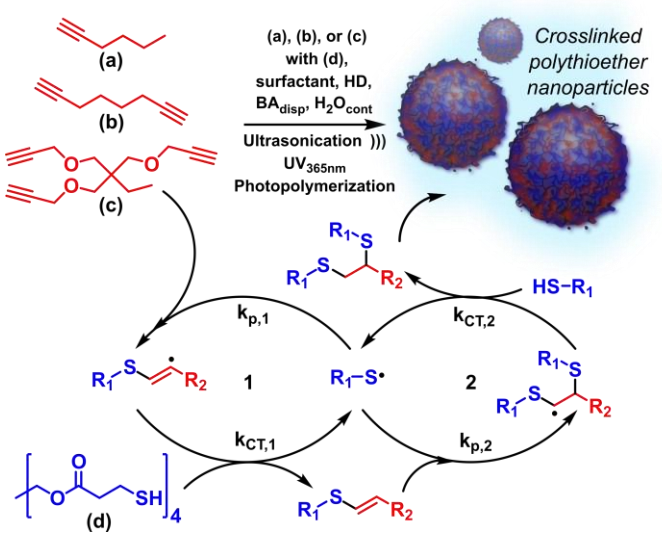

Figure 16. Thiol-alkyne photopolymerization in miniemulsion for nanoparticle synthesis.

and cured with ultraviolet light. The resulting emulsions were analysed *via* dynamic light scattering, transmission electron microscopy as well as atomic force microscopy. Light scattering data over a wide range of organic volume fractions was performed to optimize the size of the resulting nanoparticles, as shown in Figure 17. The smallest mean particle size was obtained with 2.25 vol.% with 80, 62, and 55 nm for TMPTPE, 1-hexyne, and 1,7-octadiyne respectively. Representative AFM images of nanoparticles prepared from

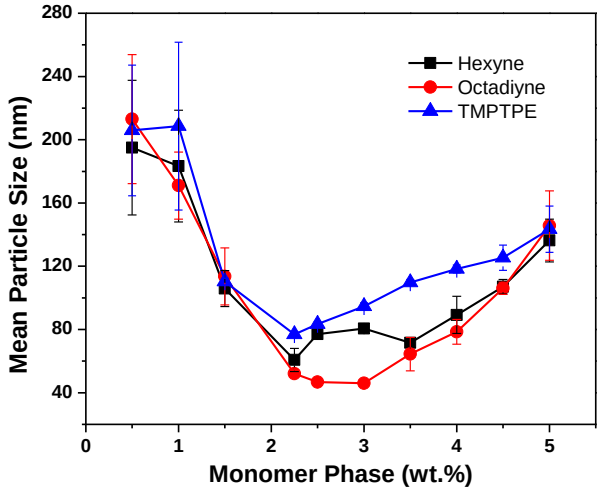

Figure 17. Size dependence on organic (monomer) phase wt.% in thiol-yne nanoparticles.

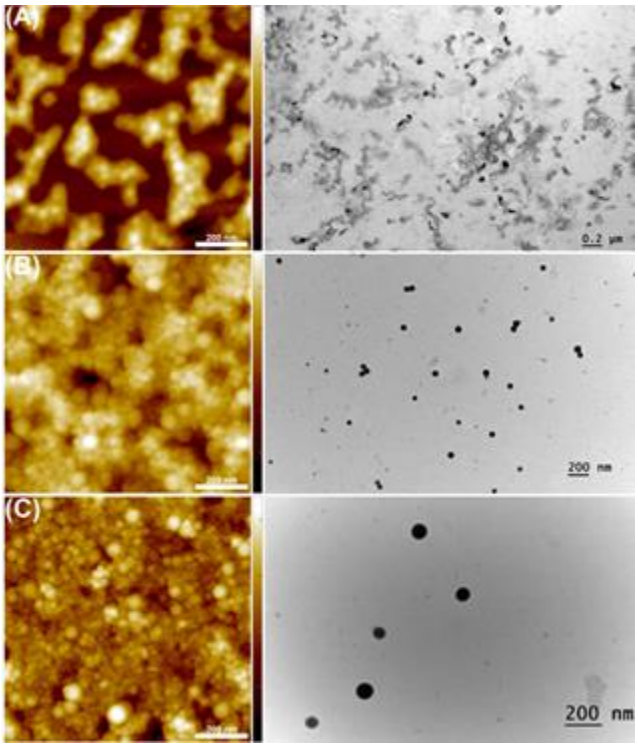

Figure 18. AFM and TEM images corresponding to (a) hexyne-PETMP, (b) 1,7-octadiyne-PETMP, and (c) TMPTPE-PETMP particles. All scale bars are 200 nm.

the three monomers with different degrees of functionality are shown in Figure 18. As shown, the higher functionality of alkyne monomers resulted in better-defined nanospheres. Upon drying, the samples with higher crosslink density proved less likely to coalesce with neighbouring particles. This phenomenon was also corroborated with TEM images, which show a mixture of coalesced nanoparticles with the 1-hexyne particles and independent spheres for the 1,7-octadiyne and TMPTPE samples.

Next, the thermal properties of thiol-alkyne nanoparticles were studied as a function of varying alkyne monomers. The results obtained from differential scanning calorimetry (DSC) are shown in Figure 19. As expected, nanoparticles obtained from hexyne-PETMP displayed the lowest glass transition temperature (T_g) at -32.5 °C because of the low crosslink density obtained from the monofunctional alkyne. Increasing the alkyne functionality to two or three alkynes using either 1,7-octadiyne or TMPTPE,

respectively, provided nanoparticles with higher T_g. Nanoparticles derived from 1,7-octadiyne exhibited a T_g at 45.7 °C, while nanoparticles derived from TMPTPE displayed a T_g at 47.3 °C. These results are consistent with an expected increase in T_g with an increase in network crosslink density at higher alkyne functionality.

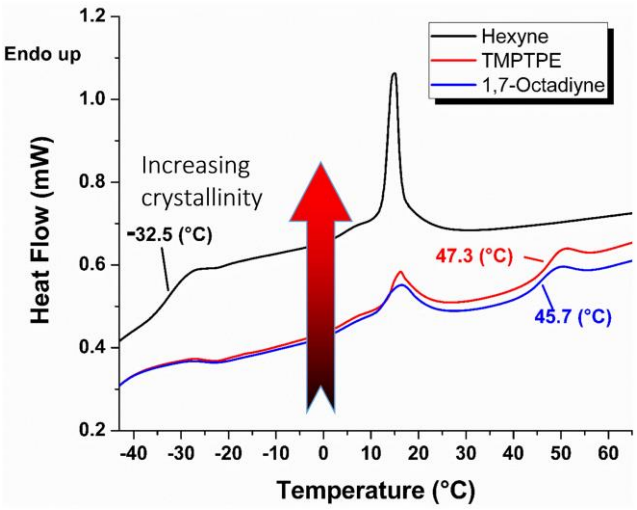

Figure 19. DSC plot of alkyne monomers with varying functionality.

To fully exploit the thiol-yne system, different stoichiometries of thiol and alkyne were reacted within the miniemulsions. Fourier transform infrared spectroscopy was used to analyse the conversion of the functional groups as the ratios of SH to alkyne were adjusted from 1:1, 2:1, and 4:1 (Figure 20). The disappearance of both the SH and alkyne peaks at 3285 cm^{-1} and 2567 cm^{-1} respectively for the 2:1 SH:yne, demonstrates that conversion of the functional groups to near one hundred percent conversion. When the alkyne is in excess (1:1, SH:yne) a strong alkyne absorption remained. Additionally the excess SH (4:1 SH:yne) shows the presence of residual mercaptan functionality.

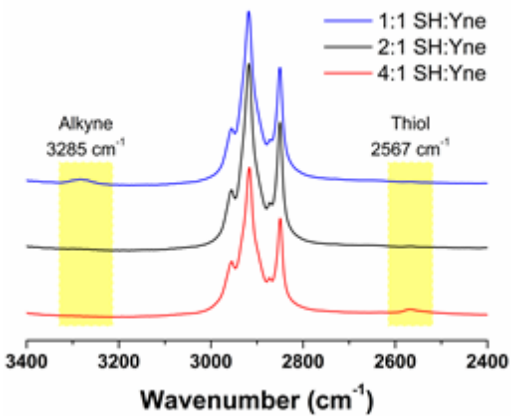

Figure 20. FT-IR spectra of miniemulsions prepared with different ratios of SH:yne for the 1,7-octadiyne sample.

To illustrate the ease of orthogonal click reactions, fluorescent dyes were ligated on the nanoparticle surface *via* both thiol-yne and alkyne-azide click reactions. To the excess SH nanoparticles (4:1 SH:yne), Texas Red maleimide was attached through a thiol-Michael click reaction which resulted in fluorescently tagged nanoparticles (Figure 21a). To the excess alkyne nanoparticles, the UV activated thiol-yne reaction was carried out in the in the presence of 2,2-dimethoxy-2-phenylacetophenone and 7-mercapto-4-methylcoumarin to afford fluorescently labelled nanoparticles (Figure 21b). It is important to demonstrate the ability of other potential reactions to improve the usefulness of this platform. The copper(I)-catalyzed azide-alkyne cycloaddition (CuAAC) click reaction between Alexa Fluor® 488 Azide and the excess yne nanoparticles resulted in green fluorescently tagged nanoparticles (Figure 21c). The functionalization of the nanoparticles through three different "click" reactions successfully demonstrates the versatility of the particles as a platform for the rapid preparation of easy to functionalize nanoparticles. The successful covalent attachment of all fluorescent dyes on the surface of the nanoparticles was confirm using fluorescence microscopy, as shown in Figure 22.

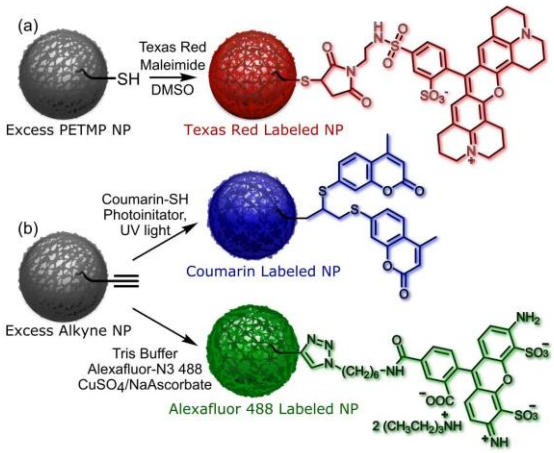

Figure 21. (a) Thiol-functional polythioether nanoparticles prepared with excess PETMP and postmodified *via* thiol-Michael with Texas Red maleimide. (b) Alkyne-functional polythioether nanoparticles prepared with excess 1,7-octadiyne postmodified with 7-mercapto-4-methylcoumarin *via* thiol-yne or with Alexa Fluor® 488 Azide *via* CuAAC.

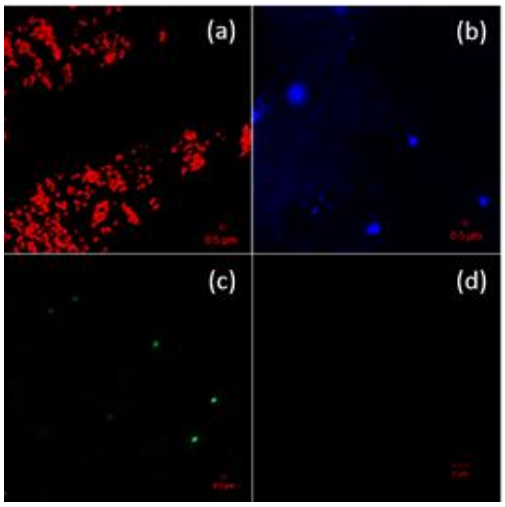

Figure 22. Fluorescence microscopy of (a) thiol-functional nanoparticles postmodified with Texas Red maleimide using a thiol-Michael reaction, (b) alkyne-functional nanoparticles modified by photoinitiated thiol-yne with 7-mercapto-4-methylcoumarin, and (c) alkyne-functional nanoparticles postmodified by CuAAC with Alexa Fluor® 488 Azide. (d) shows a control experiment with non-reactive dyes.

Lastly, thiol–yne photopolymerization was utilized as a rapid two-step synthetic approach to prepare silver–polythioether nanoparticles. First, hydrophobically modified AgNPs were prepared via sodium borohydride reduction of silver nitrate in the presence of dodecanethiol, which yielded 9 ± 3 nm AgNPs with a λ_{max} = 435 nm. After

purification, the AgNPs were dispersed in BA and combined with the thiol–alkyne monomer formulation. The reaction mixture was then ultrasonicated in the presence of water and SDS, and polymerized with ultraviolet light for 20 minutes to yield composite Ag–polythioether nanoparticles. This photopolymerization methodology markedly improves upon current thermal miniemulsion routes, which typically require 4–24 h reaction time to yield composite nanoparticles. TEM analysis revealed well-defined core–shell particle morphologies with AgNPs strictly confined within the core of the polythioether nanoparticles. Image analysis carried out on a population of nanoparticles imaged at 50 keV revealed an average composite diameter of 127 ± 8 nm, an average inorganic core diameter of 68 ± 6 nm, and a clearly defined polythioether shell of around 30 nm. Additional TEM images collected at 200 keV showed that the inorganic core was comprised of multiple individual AgNPs. The results are shown below in Figure 23.[21]

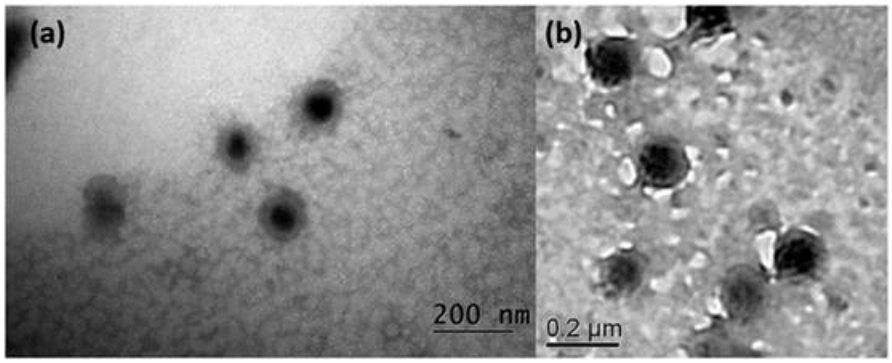

Figure 23. Representative TEM micrographs of composite polythioether–silver nanoparticles collected at (a) 50 keV and (b) 200 keV, showing clusters of 9 nm AgNPs encapsulated within 1,7-octadiyne-PETMP nanoparticles.

Chapter V. Conclusion

In this thesis, I have elucidated the design parameters necessary for the effective utilization of thiol-ene and thiol-yne photopolymerization techniques in miniemulsion. The outcomes of this research provide simple synthetic strategies based on thiol-ene/yne photopolymerization in miniemulsion that enable the fabrication of polythioether nanoparticles with the ability to encapsulate useful compounds such as silver for potential applications as antimicrobial materials. Nanoparticle size and distribution are tunable via judicious choice of formulation parameters and processing conditions. Synthesis of polythioether nanoparticles under non-stoichiometric conditions provides thiol, alkene, or alkyne functional surfaces and enables one-pot postpolymerization modification

References

1. Rao, J. P.; Geckeler, K. E., Polymer nanoparticles: Preparation techniques and size-control parameters. *Prog. Polym. Sci.* **2011,** *36* (7), 887-913.
2. Asua, J. M., Miniemulsion polymerization. *Prog. Polym. Sci.* **2002,** *27* (7), 1283-1346.
3. Landfester, K., Miniemulsion Polymerization and the Structure of Polymer and Hybrid Nanoparticles. *Angew. Chem. Int. Ed.* **2009,** *48* (25), 4488-4507.
4. Solans, C.; Izquierdo, P.; Nolla, J.; Azemar, N.; Garcia-Celma, M. J., Nano-emulsions. *Curr. Opin. Colloid Interface Sci.* **2005,** *10* (3), 102-110.
5. Hecht, L. L.; Wagner, C.; Landfester, K.; Schuchmann, H. P., Surfactant concentration regime in miniemulsion polymerization for the formation of MMA nanodroplets by high-pressure homogenization. *Langmuir* **2011,** *27* (6), 2279-2285.
6. Tiarks, F.; Landfester, K.; Antonietti, M., Preparation of polymeric nanocapsules by miniemulsion polymerization. *Langmuir* **2001,** *17* (3), 908-918.
7. Bon, S. A.; Colver, P. J., Pickering miniemulsion polymerization using laponite clay as a stabilizer. *Langmuir* **2007,** *23* (16), 8316-8322.
8. Liu, Z.; Lu, Y.; Zhang, M.; Wan, W.; Luo, G., Controllable preparation of uniform polystyrene nanospheres with premix membrane emulsification. *J. Appl. Polym. Sci.* **2013,** *129* (3), 1202-1211.
9. Joscelyne, S. M.; Tragardh, G., Membrane emulsification - a literature review. *J. Membrane Sci.* **2000,** *169* (1), 107-117.
10. Nazir, A.; Schroen, K.; Boom, R., Premix emulsification: A review. *J. Membrane Sci.* **2010,** *362* (1-2), 1-11.
11. Antonietti, M.; Landfester, K., Polyreactions in miniemulsions. *Prog. Polym. Sci.* **2002,** *27* (4), 689-757.
12. Crespy, D.; Landfester, K., Miniemulsion polymerization as a versatile tool for the synthesis of functionalized polymers. *Beilstein J. Org.Chem.* **2010,** *6*, 1132-1148.
13. Landfester, K.; Tiarks, F.; Hentze, H.-P.; Antonietti, M., Polyaddition in miniemulsions: A new route to polymer dispersions. *Macromol. Chem. Phys.* **2000,** *201* (1), 1-5.
14. Tiarks, F.; Landfester, K.; Antonietti, M., One-step preparation of polyurethane dispersions by miniemulsion polyaddition. *J. Polym. Sci. Part A: Polym. Chem.* **2001,** *39* (14), 2520-2524.
15. Siebert, J. M.; Baier, G.; Musyanovych, A.; Landfester, K., Towards copper-free nanocapsules obtained by orthogonal interfacial "click" polymerization in miniemulsion. *Chem. Commun.* **2012,** *48* (44), 5470-5472.
16. Roux, R.; Sallet, L.; Alcouffe, P.; Chambert, S.; Sintes-Zydowicz, N.; Fleury, E.; Bernard, J., Facile and Rapid Access to Glyconanocapsules by CuAAC Interfacial Polyaddition in Miniemulsion Conditions. *ACS Macro Lett.* **2012,** *1* (8), 1074-1078.
17. Hoyle, C. E.; Lee, T.; Roper, T., Thiol-enes: Chemistry of the past with promise for the future. *J. Polym. Sci. Part A: Polym. Chem.* **2004,** *42* (21), 5301-5338.
18. Hoyle, C. E.; Bowman, C. N., Thiol-ene click chemistry. *Angew. Chem. Int. Ed.* **2010,** *49* (9), 1540-1573.

19. Hoyle, C. E.; Lowe, A. B.; Bowman, C. N., Thiol-click chemistry: A multifaceted toolbox for small molecule and polymer synthesis. *Chem. Soc. Rev.* **2010,** *39* (4), 1355-1387.
20. van Berkel, K. Y.; Hawker, C. J., Tailored composite polymer–metal nanoparticles by miniemulsion polymerization and thiol-ene functionalization. *J. Polym. Sci. Part A: Polym. Chem.* **2010,** *48* (7), 1594-1606.
21. Zou, J.; Hew, C. C.; Themistou, E.; Li, Y.; Chen, C.-K.; Alexandridis, P.; Cheng, C., Clicking Well-Defined Biodegradable Nanoparticles and Nanocapsules by UV-Induced Thiol-Ene Cross-Linking in Transparent Miniemulsions. *Adv. Mater.* **2011,** *23* (37), 4274-4277.
22. Durham, O. Z.; Krishnan, S.; Shipp, D. A., Polymer Microspheres Prepared by Water-Borne Thiol–Ene Suspension Photopolymerization. *ACS Macro Lett.* **2012,** *1* (9), 1134-1137.
23. Durham, O. Z.; Shipp, D. A., Suspension thiol-ene photopolymerization: Effect of stabilizing agents on particle size and stability. *Polymer* **2014,** *55* (7), 1674-1680.
24. Tan, J.; Li, C.; Zhou, J.; Yin, C.; Zhang, B.; Gu, J.; Zhang, Q., Fast and facile fabrication of porous polymer particles via thiol–ene suspension photopolymerization. *RSC Adv.* **2014,** *4* (26), 13334.
25. Jasinski, F.; Lobry, E.; Tarablsi, B.; Chemtob, A.; Croutxé-Barghorn, C.; Le Nouen, D.; Criqui, A., Light-Mediated Thiol–Ene Polymerization in Miniemulsion: A Fast Route to Semicrystalline Polysulfide Nanoparticles. *ACS Macro Lett.* **2014,** *3* (9), 958-962.
26. Wang, C.; Podgórski, M.; Bowman, C. N., Monodisperse functional microspheres from step-growth "click" polymerizations: preparation, functionalization and implementation. *Mater. Horiz.* **2014**.
27. Amato, D. V.; Amato, D. N.; Flynt, A. S.; Patton, D. L., Functional, sub-100 nm polymer nanoparticles via thiol-ene miniemulsion photopolymerization. *Polymer Chemistry* **2015,** *6* (31), 5625-5632.
28. Chan, J. W.; Zhou, H.; Hoyle, C. E.; Lowe, A. B., Photopolymerization of Thiol-Alkynes: Polysulfide Networks. *Chem. Mater.* **2009,** *21* (8), 1579-1585.
29. Lowe, A. B.; Hoyle, C. E.; Bowman, C. N., Thiol-yne click chemistry: A powerful and versatile methodology for materials synthesis. *J. Mater. Chem.* **2010,** *20* (23), 4745-4750.
30. Fairbanks, B. D.; Scott, T. F.; Kloxin, C. J.; Anseth, K. S.; Bowman, C. N., Thiol-Yne Photopolymerizations: Novel Mechanism, Kinetics, and Step-Growth Formation of Highly Cross-Linked Networks. *Macromolecules* **2009,** *42* (1), 211-217.
31. Chan, J. W.; Shin, J.; Hoyle, C. E.; Bowman, C. N.; Lowe, A. B., Synthesis, Thiol−Yne "Click" Photopolymerization, and Physical Properties of Networks Derived from Novel Multifunctional Alkynes. *Macromolecules* **2010,** *43* (11), 4937-4942.
32. Gokmen, M. T.; Brassinne, J.; Prasath, R. A.; Du Prez, F. E., Revealing the nature of thio-click reactions on the solid phase. *Chem. Commun.* **2011,** *47* (16), 4652-4654.
33. Prasath, R. A.; Gokmen, M. T.; Espeel, P.; Du Prez, F. E., Thiol-ene and thiol-yne chemistry in microfluidics: a straightforward method towards macroporous and nonporous functional polymer beads. *Polym. Chem.* **2010,** *1* (5), 685-692.
34. Amato, D. N.; Amato, D. V.; Narayanan, J.; Donovan, B. R.; Douglas, J. R.; Walley, S. E.; Flynt, A. S.; Patton, D. L., Functional, composite polythioether

nanoparticles via thiol-alkyne photopolymerization in miniemulsion. *Chem. Commun.* **2015,** *51* (54), 10910-10913.
35. Lipinski, C. A., Drug-like properties and the causes of poor solubility and poor permeability. *J. Pharmacol. Toxicol. Methods* **2000,** *44* (1), 235-249.
36. Koo, O. M.; Rubinstein, I.; Onyuksel, H., Role of nanotechnology in targeted drug delivery and imaging: a concise review. *Nanomed. Nanotechnol. Biol. Med.* **2005,** *1* (3), 193-212.
37. Davis, M. E.; Chen, Z.; Shin, D. M., Nanoparticle therapeutics: an emerging treatment modality for cancer. *Nat Rev Drug Discov* **2008,** *7* (9), 771-782.
38. Parveen, S.; Misra, R.; Sahoo, S. K., Nanoparticles: a boon to drug delivery, therapeutics, diagnostics and imaging. *Nanomedicine: Nanotechnology, Biology and Medicine* **2012,** *8* (2), 147-166.
39. Ge, Z.; Liu, S., Functional block copolymer assemblies responsive to tumor and intracellular microenvironments for site-specific drug delivery and enhanced imaging performance. *Chem. Soc. Rev.* **2013,** *42* (17), 7289-7325.
40. Farrell, Z.; Shelton, C.; Dunn, C.; Green, D., Straightforward, One-Step Synthesis of Alkanethiol-capped Silver Nanoparticles from an Aggregative Model of Growth. *Langmuir* **2013,** *29* (30), 9291-9300.
41. Brown, J. C.; Pusey, P. N.; Dietz, R., Photon correlation study of polydisperse samples of polystyrene in cyclohexane. *J. Chem. Phys.* **1975,** *62* (3), 1136-1144.
42. Jenkins, P.; Snowden, M., Depletion flocculation in colloidal dispersions. *Adv. Colloid Interfac.* **1996,** *68* (0), 57-96.
43. Kiratzis, N.; Faers, M.; Luckham, P. F., Depletion flocculation of particulate systems induced by hydroxyethylcellulose. *Colloids and Surfaces A: Physicochemical and Engineering Aspects* **1999,** *151* (3), 461-471.